GEOPHYSICS, VOL. 80, NO. 6 (NOVEMBER-DECEMBER 2015); P. EN167–EN177, 5 FIGS., 1 TABLE.
10.1190/GEO2014-0612.1

Nonperturbational surface-wave inversion: A Dix-type relation for surface waves

Matthew M. Haney[1] and Victor C. Tsai[2]

ABSTRACT

We extend the approach underlying the well-known Dix equation in reflection seismology to surface waves. Within the context of surface wave inversion, the Dix-type relation we derive for surface waves allows accurate depth profiles of shear-wave velocity to be constructed directly from phase velocity data, in contrast to perturbational methods. The depth profiles can subsequently be used as an initial model for nonlinear inversion. We provide examples of the Dix-type relation for under-parameterized and over-parameterized cases. In the under-parameterized case, we use the theory to estimate crustal thickness, crustal shear-wave velocity, and mantle shear-wave velocity across the Western U.S. from phase velocity maps measured at 8-, 20-, and 40-s periods. By adopting a thin-layer formalism and an over-parameterized model, we show how a regularized inversion based on the Dix-type relation yields smooth depth profiles of shear-wave velocity. In the process, we quantitatively demonstrate the depth sensitivity of surface-wave phase velocity as a function of frequency and the accuracy of the Dix-type relation. We apply the over-parameterized approach to a near-surface data set within the frequency band from 5 to 40 Hz and find overall agreement between the inverted model and the result of full nonlinear inversion.

INTRODUCTION

Dix (1955) derived an approximate but widely used method of inversion of stacking velocities, computed from reflections at discrete interfaces, for the velocities of the layers between the interfaces known as *interval velocities*. The method is based on the assumption that, at short offsets, the stacking velocity of the nth interface $V_{\mathrm{st},n}$ is equal to the root-mean-square (rms) velocity of the layers above the interface depth weighted by traveltimes:

$$V_{\mathrm{st},n} = \sqrt{\frac{\sum_{i=1}^{n} V_i^2 \Delta t_i}{\sum_{i=1}^{n} \Delta t_i}}, \tag{1}$$

in which V_i and Δt_i are the velocity and the vertical two-way traveltime through the ith layer, respectively. Equation 1 implies a linear relationship between the squared stacking velocities and the squared interval velocities with the approximation being based on short offsets (Taner and Koehler, 1969; Yilmaz, 1987). Dix (1955) solved equation 1 exactly for the interval velocities, and the resulting analytical expression is commonly referred to as the *Dix equation*. However, in practice, the exact solution is not robust in the presence of noise and therefore regularization must be applied to equation 1 to obtain meaningful results (Harlan, 1999; Koren and Ravve, 2006). Approaches based on the work of Dix (1955) have been extended to converted waves for the estimation of shear wave interval velocities (Stewart and Ferguson, 1997) and to anisotropy (Grechka et al., 1999).

Here, we report on an extension of the Dix technique to surface waves. By analogy with equation 1, we show that surface-wave phase velocity is the counterpart of stacking velocity, and the shear wave velocity of a layer is the counterpart of interval velocity. Instead of weighting with traveltime, as in equation 1, the weighting in the surface-wave case is based on the associated eigenfunctions. The initial form of the theory we present is based on the idea of representing Rayleigh waves at each frequency as propagating in a different homogeneous half space. After deriving a Dix-type relation based on a homogeneous medium, we extend the theory to include the possibility of Rayleigh or Love waves propagating in velocity-depth profiles described by power laws. In unconsolidated granular deposits, such power-law profiles constitute a more realistic model of shear wave velocity than a homogeneous model

Manuscript received by the Editor 28 December 2014; revised manuscript received 28 April 2015; published online 16 October 2015.
[1]U.S. Geological Survey Volcano Science Center, Alaska Volcano Observatory, Anchorage, Alaska, USA. E-mail: mhaney@usgs.gov.
[2]California Institute of Technology, Seismological Laboratory, Pasadena, California, USA. E-mail: tsai@caltech.edu.

(Godin and Chapman, 2001; Bergamo and Socco, 2013; Tsai and Atiganyanun, 2014).

Although surface-wave inversion is a highly nonlinear problem (Xia et al., 1999), the Dix-type relation we derive for surface waves is linear in terms of the squared shear wave layer velocities. Thus, it can be used to generate a reliable starting model for subsequent iterative nonlinear inversion. Such an approach has not been discussed previously for surface waves, although Xia et al. (1999) present a related data-driven method for constructing a starting model for surface-wave phase velocity inversion. From the Dix-type relation for surface waves, we are able to make a connection to the starting model generation method of Xia et al. (1999). We formulate an underparameterized version of the Dix-type relation for a model of a single layer over a half-space and map crustal thickness across the western United States from phase velocity maps measured at three periods. The map of crustal thickness and values for crustal and mantle velocity agree well with what is known about crustal structure. We further develop an overparameterized Dix-type inversion and apply the method to synthetic data and field data recorded in a near-surface setting. In the process, we quantify the error inherent in our approximation and elucidate the depth sensitivities of Rayleigh and Love waves.

METHOD

Fundamental-mode Rayleigh waves

We first consider the dispersion of fundamental-mode Rayleigh waves. Equation 7.75 in Aki and Richards (1980) states that a Rayleigh-wave eigenfunction satisfies

$$\omega^2 I_1 - k^2 I_2 - k I_3 - I_4 = 0, \tag{2}$$

where I_1, I_2, I_3, and I_4 are given by

$$I_1 = \frac{1}{2}\int_0^\infty \rho(r_1^2 + r_2^2)dz, \tag{3}$$

$$I_2 = \frac{1}{2}\int_0^\infty [(\lambda + 2\mu)r_1^2 + \mu r_2^2]dz, \tag{4}$$

$$I_3 = \int_0^\infty \left(\lambda r_1 \frac{\partial r_2}{\partial z} - \mu r_2 \frac{\partial r_1}{\partial z}\right)dz, \tag{5}$$

$$I_4 = \frac{1}{2}\int_0^\infty \left[(\lambda + 2\mu)\left(\frac{\partial r_2}{\partial z}\right)^2 + \mu\left(\frac{\partial r_1}{\partial z}\right)^2\right]dz, \tag{6}$$

in which ρ is the density, λ is Lamé's first parameter, and μ is the shear modulus. In equations 3–6, r_1 and r_2 represent the horizontal and vertical Rayleigh-wave displacement eigenfunctions. For a given frequency ω, equation 2 leads to a generalized quadratic eigenvalue/eigenvector equation in terms of the wavenumber k, and the eigenfunctions r_1 and r_2.

Classical Rayleigh-wave inversion proceeds, as described by Aki and Richards (1980), by perturbing equation 2 and finding a linearized relation between the perturbation in phase velocity $c = \omega/k$ and perturbations in the material properties ρ, λ, and μ. The inversion is nonlinear and involves iteratively adjusting an initial model until convergence is obtained.

By adopting some approximations, a more straightforward type of inversion can be realized for the fundamental Rayleigh mode. In contrast to the classical method, this approximate method is not based on perturbations. The idea is based on using an approximate eigenfunction in equation 2 and solving for phase velocity. A similar approach based on approximate eigenfunctions was used by Tsai et al. (2012) in their evaluation of surface-wave scaling for a power-law velocity profile. The approximation we use is based on Rayleigh's principle. This principle states that when there is a perturbation in medium properties, the eigenvalue change is of first order in terms of the medium property change, whereas the change in the eigenfunction is at least a second-order effect (Snieder and Trampert, 1999). As described below, the method we develop matches the eigenvalue, or phase velocity, at a given frequency but uses an approximate eigenfunction. The approximation is exact to first order in the limit of a weakly heterogeneous velocity profile. Away from this limit, the approximation becomes worse but still provides a reasonable solution. Our initial approximate eigenfunctions result from the assumption that, at a given frequency ω, the Rayleigh wave propagates in a homogeneous medium with constant density, a Poisson's ratio of 0.25 ($\lambda = \mu$), and a shear velocity that is a factor of 0.9194^{-1} times the observed phase velocity at that frequency. Note that the method can be formulated for other values of Poisson's ratio; however, we choose a value of 0.25 for illustrative purposes. With these assumptions, at each frequency, the Rayleigh wave is assumed to be propagating in a different homogeneous medium. This procedure is similar to the approximation of a homogeneous medium with velocity equal to the rms velocity overlying a layer in the Dix equation (Dix, 1955). Because the medium we consider is homogeneous, the eigenfunctions are known analytically (Lay and Wallace, 1995):

$$r_1(z) = e^{-0.8475kz} - 0.5773e^{-0.3933kz} \tag{7}$$

$$r_2(z) = 0.8475e^{-0.8475kz} - 1.4679e^{-0.3933kz}. \tag{8}$$

We take the subsurface model to be inverted for as made up of N uniform layers each with a different shear velocity β. Layer 1 extends from depth h_1 to h_2, and so on. For simplicity, the depth at the top of the model h_1 is set to 0. Layer N, the deepest layer, extends from h_N to infinite depth. Inserting this depth model into equations 2–6, along with equations 7 and 8, the assumption of constant density and a Poisson's ratio of 0.25, results in the following relation upon performing the integrals analytically:

$$c_m^2 = \frac{\sum_{n=1}^{N}\left[-3.5305e^{-1.6950k_m z} + 7.8286e^{-1.2408k_m z} - 5.3471e^{-0.7866k_m z}\right]_{h_n}^{h_{n+1}}\beta_n^2}{\sum_{n=1}^{N}\left[-1.0137e^{-1.6950k_m z} + 2.9358e^{-1.2408k_m z} - 3.1630e^{-0.7866k_m z}\right]_{h_n}^{h_{n+1}}}, \tag{9}$$

where the expressions in brackets are evaluated at the deepest depth h_{n+1} minus the shallowest depth h_n of the nth layer. Note that subscript m in equation 9 represents the mth frequency at which a phase velocity measurement is available and $k_m = \omega_m/c_m$. Only the $h_1 = 0$ term of the summation in the denominator survives the sum over the layers. This leads to a factor of 1.2409 in the denominator, yielding

$$c_m^2 = \sum_{n=1}^{N} [-2.8450e^{-1.6950k_m z} + 6.3086e^{-1.2408k_m z} - 4.3089e^{-0.7866k_m z}]_{h_n}^{h_{n+1}} \beta_n^2. \quad (10)$$

Denoting the function in the brackets by $f(k_m, z)$, this equation is further simplified as

$$c_m^2 = \sum_{n=1}^{N} [f(k_m, h_{n+1}) - f(k_m, h_n)]\beta_n^2, \quad (11)$$

where $f(k_m, h_1 = 0) = -0.8453 = -f_0$. Equation 11 can be represented as a matrix-vector relationship between the squared phase velocities and the squared shear velocities of the layers:

$$\vec{c^2} = \mathbf{G}\vec{\beta^2}, \quad (12)$$

where $\mathbf{G}$ is a matrix of size $M \times N$ with M being the number of phase velocity measurements and N being the number of layers. In the formulation of equation 12, the depths of the layer boundaries are set, and only the shear velocities of the layers are unknown. The relation between the squared phase velocities and the squared layer velocities is analogous to the Dix-type relation between the squared stacking velocities and squared interval velocities (Dix, 1955). Thus, by analogy, equation 12 represents a Dix-type relation for surface waves. In contrast to the Dix-type relation for reflections, the matrix $\mathbf{G}$ in the surface-wave case is not a lower triangular matrix. Due to the lower triangular structure of the matrix for the reflection case, the matrix can be inverted analytically yielding the exact solution known as the Dix equation (Dix, 1955). Such an analytical solution does not exist for surface waves; however, as we show in a later section, the regularized pseudoinverse of $\mathbf{G}$ displays a clear pattern that represents the depth range of surface-wave sensitivity at a given frequency.

Fundamental-mode Love waves

Our formulation of the Dix-type relation for surface waves up to this point does not work for Love waves because they do not exist in a homogeneous half space. To develop a theory for Love waves, we instead consider depth models described by power-law velocity profiles, in which Love waves exist. Such models are generic and may provide a more realistic description of the shallow subsurface than a homogeneous model in many cases (Godin and Chapman, 2001; Bergamo and Socco, 2013; Tsai and Atiganyanun, 2014). Similar to the development of the theory for Rayleigh waves, equation 7.69 in Aki and Richards (1980) states that a Love-wave eigenfunction satisfies

$$\omega^2 I_1 - k^2 I_2 - I_3 = 0, \quad (13)$$

in which I_1, I_2, and I_3 are given by

$$I_1 = \frac{1}{2}\int_0^\infty \rho l_1^2 dz, \quad (14)$$

$$I_2 = \frac{1}{2}\int_0^\infty \mu l_1^2 dz, \quad (15)$$

$$I_3 = \frac{1}{2}\int_0^\infty \mu \left(\frac{\partial l_1}{\partial z}\right)^2 dz, \quad (16)$$

and where l_1 represents the Love-wave displacement eigenfunction in equations 14–16. For a given frequency ω, equation 13 leads to a generalized eigenvalue/eigenvector equation in terms of the squared wavenumber k^2 and l_1.

To develop the Dix-type relation for Love waves, we need an approximate eigenfunction for power-law velocity profiles. We consider an exponential approximation, $l_1 \sim e^{-akz}$, as is also used by Tsai et al. (2012). By fitting this functional form to the exact Love-wave eigenfunctions over a range of realistic power-law velocity profiles described by $\beta(z) \sim z^\alpha$ for $\alpha \in [0.250 \quad 0.275 \quad 0.300 \quad 0.325 \quad 0.350 \quad 0.375 \quad 0.400]$, we find that $a = 0.85 \pm 0.09$. Proceeding as in the Rayleigh-wave case, we insert this approximate eigenfunction into equations 13–16 along with a layered depth model and find, upon performing the integrals analytically, that

$$c_m^2 = (1 + a^2)\sum_{n=1}^{N} (e^{-2ak_m h_n} - e^{-2ak_m h_{n+1}})\beta_n^2, \quad (17)$$

which is the analog of equation 10. Denoting the function $f(k_m, z) = -(1 + a^2)e^{-2ak_m z}$ for the case of Love waves, this equation can be put into a form identical to equation 11 for Rayleigh waves:

$$c_m^2 = \sum_{n=1}^{N} [f(k_m, h_{n+1}) - f(k_m, h_n)]\beta_n^2, \quad (18)$$

which shows that, as seen previously for Rayleigh waves, there is a matrix-vector relationship between the squared Love-wave phase velocities and the squared layer shear velocities.

Rayleigh waves in a power-law velocity profile

Because we have just considered power-law velocity profiles for Love waves, we can also develop a more advanced Dix-type relation for Rayleigh waves based on their approximate eigenfunctions in a power-law velocity profile. Guided by the forms in equations 7 and 8, we take a biexponential approximation for the horizontal eigenfunction given by $r_1 \sim C_1 e^{-a_1 kz} + C_2 e^{-a_2 kz}$ and a similar biexponential approximation for the vertical eigenfunction r_2. By fitting these functional forms to the exact Rayleigh-wave eigenfunctions over a range of realistic power-law velocity profiles as discussed previously for Love waves, we find the constants for the biexponential approximations as shown in Table 1. With these approximations, we proceed as we did previously for Rayleigh waves and arrive at an equation identical in form to equation 11, except that the function in brackets $f(k_m, z)$ is given by the following equation:

$$\begin{aligned} f(k_m, z) = &-103.14e^{-1.8586k_m z} + 6.1446e^{-1.7714k_m z} \\ &+ 217.12e^{-1.7555k_m z} - 10.312e^{-1.7012k_m z} \\ &- 160.68e^{-1.6842k_m z} + 1.2856e^{-1.6683k_m z} \\ &- 115.00e^{-1.6524k_m z} + 294.66e^{-1.6140k_m z} \\ &+ 4.0924e^{-1.5981k_m z} - 135.49e^{-1.5438k_m z}. \end{aligned} \quad (19)$$

Note that the biexponential fits in Table 1 assume a Poisson's ratio equal to 0.25, although the coefficients do not vary greatly for other realistic values of Poisson's ratio.

INVERSION WITH AN UNDERPARAMETERIZED MODEL

Here, we consider a simple modification of equation 11 for a model of a single layer over a half space in which the thickness of the layer is not assumed to be known. In contrast to the case when the layer boundaries are fixed, this problem is nonlinear due to the dependence on the unknown depth of the layer. For this underparameterized model, there are three unknowns, β_1, h_2, and β_2, and a model can be determined by three or more phase-velocity measurements. This scenario is applicable for finding the thickness of a shallow, unconsolidated layer above bedrock or, at a larger scale, the thickness of the earth's crust. Surface-wave dispersion has traditionally been one of the key data sets for determining the thickness of the earth's crust (Evison et al., 1959). In a later section, we contrast this approach with an overparameterized model composed of many thin layers whose boundaries are fixed.

For ease of notation, let $f(k_m, h_2) = f_m$. Here, we adopt the homogeneous medium formulation to define f using equation 10. Then, the equations resulting from equation 11 evaluated at the three frequencies of observation are as follows:

$$c_1^2 = f_0\beta_1^2 + f_1(\beta_1^2 - \beta_2^2), \tag{20}$$

$$c_2^2 = f_0\beta_1^2 + f_2(\beta_1^2 - \beta_2^2), \tag{21}$$

$$c_3^2 = f_0\beta_1^2 + f_3(\beta_1^2 - \beta_2^2). \tag{22}$$

Solving equations 20 and 21 for β_1^2 and β_2^2 results in

$$\beta_1^2 = \frac{f_2c_1^2 - f_1c_2^2}{f_0(f_2 - f_1)}, \tag{23}$$

$$\beta_2^2 = \beta_1^2 + \frac{c_1^2 - c_2^2}{f_2 - f_1}. \tag{24}$$

Substituting equations 23 and 24 into equation 22 results in

$$0 = (f_2 - f_3)c_1^2 + (f_3 - f_1)c_2^2 + (f_1 - f_2)c_3^2, \tag{25}$$

which is a nonlinear equation in terms of the thickness of the layer only. By scanning over possible thicknesses and finding the thickness that minimizes the absolute value of the expression on the right side of equation 25, the thickness of the layer can be estimated. This estimate of the thickness can in turn be inserted into equations 23 and 24 to find estimates of the shear velocities of the layer and half-space. To select a thickness as the optimal value, we additionally require that the resulting velocities computed from equations 23 and 24 are real valued.

In Figure 1, we show the result of this inversion methodology for an underparameterized model at the continental scale. We use phase velocity maps of the western United States at 8-, 20-, and 40-s periods constructed by Lin et al. (2008, 2009) from ambient noise correlations. The phase velocity maps of Lin et al. (2008, 2009) use the dense USArray Transportable Array deployment of more than 800 stations and exist on a grid of $0.2° \times 0.2°$. Eikonal tomography (Lin et al., 2009) of the measured phase traveltimes derived from ambient noise correlations at each period yields the phase velocity maps. From these three phase velocity measurements, crustal thickness, crustal shear wave velocity, and mantle shear wave velocity can be found by applying equations 23–25. Figure 1a and 1b shows a map and histogram of the estimated crustal thickness. Several features in Figure 1a agree with known crustal structure of the western United States, including the thick crust beneath the central Rocky Mountains and the thin crust in the Basin and Range province (Chulick and Mooney, 2002). The histogram in Figure 1b shows a thickness distribution peaked at 36 km, close to the average thickness of the North American crust found by Chulick and Mooney (2002) to be 36.7 km. This depth is also close to the crust-mantle interface at 35 km in the IASP91 model (Kennett and Engdahl, 1991). Figure 1c-1f depicts the results for crustal and upper mantle shear wave velocity, with a clear indication of an overall approximately 25% contrast in shear wave velocity between the crust and mantle. This velocity contrast between the crust and upper mantle is also supported by the IASP91 model (Kennett and Engdahl, 1991). In Figure 1e, the Yellowstone hotspot (YH) track is clearly imaged as a low shear wave velocity zone in the upper mantle. Such widespread imaging of crustal thickness, crustal shear wave velocity, and mantle shear wave velocity can be used in other areas with dense networks of seismometers. Although this example is at the continental scale, we expect the theory will apply in other settings in which the surface waveguide can be approximated as a single layer.

INVERSION WITH AN OVERPARAMETERIZED MODEL

Returning to equation 12, we now consider an inversion model composed of many thin layers. Such an approach, when applied to the modeling of surface-wave dispersion, is known as the *thin-layer method* (Lysmer, 1970; Kausel, 2005; Haney et al., 2010). When applied to inversion, this is an overparameterized method in which a choice of regularization leads to a preferentially smooth model. A

Table 1. Mean coefficients and their standard deviation for the fit of a biexponential model to the horizontal r_1 and vertical r_2 Rayleigh-wave displacement eigenfunctions over a range of power-law shear velocity profiles described by $\beta(z) \sim z^\alpha$ for $\alpha \in [0.250 \quad 0.275 \quad 0.300 \quad 0.325 \quad 0.350 \quad 0.375 \quad 0.400]$. These biexponential fits assume a Poisson's ratio equal to 0.25. The biexponential model is given by $C_1e^{-a_1kz} + C_2e^{-a_2kz}$. Note that because eigenfunctions are determined up to a constant multiplier, the C_1 coefficient for r_1 has been set to unity.

Eigenfunction	a_1	a_2	C_1	C_2
r_1	0.8421 ± 0.0426	0.7719 ± 0.0372	1.0000 ± 0.0000	-0.8929 ± 0.0101
r_2	0.9293 ± 0.0428	0.8262 ± 0.0316	0.8554 ± 0.0841	-0.9244 ± 0.0855

similar type of constrained inversion has been presented within the context of the classical Dix equation in reflection seismology to obtain smooth interval velocities (Harlan, 1999). We describe the regularized inversion for the matrix-vector relationship between surface-wave phase velocity and the depth profile of shear wave velocity as given in equation 12.

We adopt a method for regularizing the linear inversion problem based on weighted-damped least squares. Data covariance and model covariance matrices $\mathbf{C}_d$ and $\mathbf{C}_m$ are chosen as in Gerstoft et al. (2006). The data covariance matrix is assumed to be a diagonal matrix

$$\mathbf{C}_d = \sigma_d^2 I, \tag{26}$$

where I is the identity matrix and σ_d is the data standard deviation. For simplicity, the standard deviation is assumed to be the same for all data points (i.e., all phase velocity measurements). The model covariance matrix has the form

$$\mathbf{C}_m(i,j) = \sigma_m^2 \exp(-|z_i - z_j|/\ell), \tag{27}$$

where σ_m is the model standard deviation, z_i and z_j are the depths at the top of the ith and jth layers, and ℓ is a smoothing distance.

With the covariance matrices so chosen, the inversion proceeds by forming an augmented version of equation 12 (Snieder and Trampert, 1999; Aster et al., 2004):

$$\begin{bmatrix} \mathbf{C}_d^{-1/2}\mathbf{G} \\ \mathbf{C}_m^{-1/2} \end{bmatrix} \vec{\beta}^2 = \begin{bmatrix} \mathbf{C}_d^{-1/2}\vec{c}^2 \\ \mathbf{C}_m^{-1/2}\vec{\beta}_0^2 \end{bmatrix}, \tag{28}$$

where $\vec{c}^2$ is the phase velocity data and β_0^2 is the shear wave velocity of a half-space model whose surface-wave velocity is equal to the maximum value of the measured phase velocity. For example, if $c_{\max}$ is the maximum value of measured phase velocity, $\beta_0 = c_{\max}/0.9194$. Note that the constraint containing β_0^2 in equation 28 is designed to force the model to be close to the half-space value β_0 in areas with poor resolution, i.e., at depths below the resolution depths of surface waves. The augmented matrix-vector relation in equation 28 can be solved for the shear wave velocity-depth profile $\vec{\beta}^2$ by least squares.

In Figure 2, we show the result of the regularized inversion for synthetic data generated for a model of a layer over a half-space. The layer is 60 m thick with an shear wave velocity of 1155 m/s. The half-space has an shear wave velocity of 1732 m/s. We keep Poisson's ratio constant throughout the model at 0.25 and use the Gardner relation (Gardner et al., 1974) to compute density from the shear wave velocity. We model the phase velocities from 3 to 13 Hz, in steps of 0.2 Hz, with the thin-layer method (Lysmer, 1970; Kausel, 2005; Haney et al., 2010), which is a finite-element variational method for solving the surface-wave dispersion problem with arbitrary accuracy. After modeling, we corrupt the synthetic phase-velocity data with 1% noise. Although this example uses 1% noise, we note that the method is robust and can handle larger amounts of noise.

We setup an inversion model consisting of 150 layers, with all layers 10-m thick except for the bottom layer, which extends to infinite depth. Although the layers are fixed, the layers are thin enough compared with the wavelengths that the inversion model acts more like a continuum whose gross properties are controlled by the regularization scheme described in equations 26 and 27. As in the previous underparameterized example, we adopt the homogeneous medium formulation in the following to define f using equation 10. With the synthetic data and the inversion model, we can construct the matrix $\mathbf{G}$ in equation 12 as shown in Figure 2a. The matrix $\mathbf{G}$ has a structure determined by the eigenfunctions at

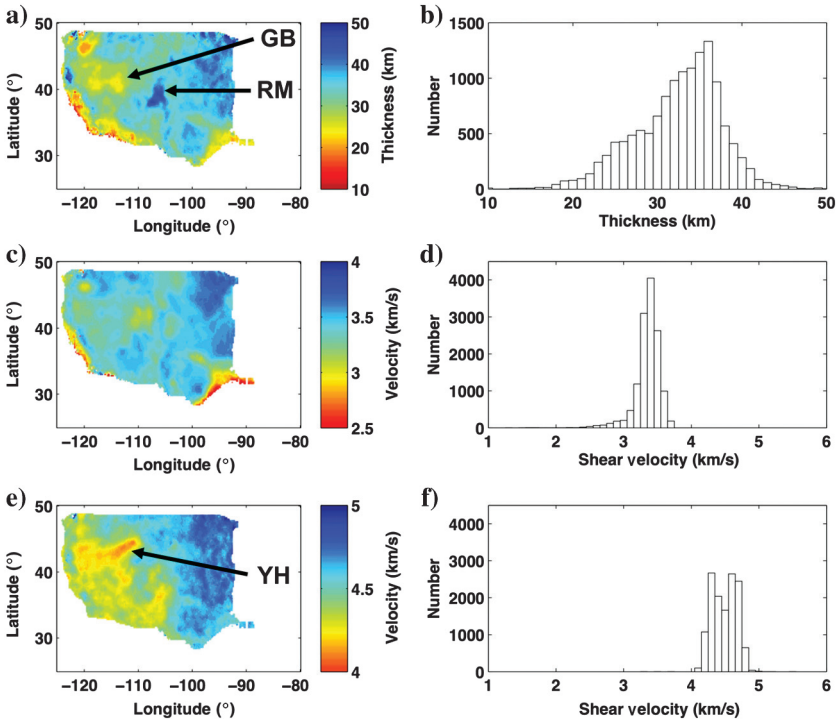

Figure 1. (a) Crustal thickness, (c) crustal shear velocity, and (e) mantle shear velocity determined from phase velocity maps at 8-, 20-, and 40-s periods across the western United States. Phase velocity maps are from Lin et al. (2008, 2009). In panel (a), the Rocky Mountain Front (RM) is clearly a region of anomalously thick crust, and the Great Basin (GB) exhibits a thin crust. Panels (b, d, and f) show histograms of the crustal thickness, crustal shear velocity, and mantle shear velocity. The distribution of crustal thicknesses peaks at 36 km in close agreement with typical 1D earth models, e.g., the Gutenberg model (Aki and Richards, 1980) and the IASP91 model (Kennett and Engdahl, 1991). Crustal and mantle shear velocities also cluster around nominal values of 3.5 and 4.5 km/s, in agreement with the Gutenberg and IASP91 models. The YH track is clearly visible in panel (e).

each frequency, with lower frequencies extending to greater depth as is normal with surface waves. We take the data and model standard deviations in equations 26 and 27 to correspond to velocities of 20 and 40 m/s, respectively, and use a smoothing length of 50 m. Note that, because the inverse problem is in terms of squared velocities, the standard deviations σ_d and σ_m are actually 400 and 1600 m^2/s^2, respectively. With these regularization parameters, we can form the regularized pseudoinverse of **G** as shown in Figure 2b. The pseudoinverse has a structure characterized by a distinctive ridge that becomes deeper with lower frequencies. This structure means that the sensitivity of phase-velocity measurements has a relatively compact depth range determined by the width of the ridge. In Figure 2b, we also plot a depth-frequency relation given by Xia et al. (1999) to construct initial models for surface-wave inversion. Xia et al. (1999) found from modeling that a Rayleigh-wave phase velocity c_R with wavelength λ could be mapped to a shear velocity of $c_R/0.88$ at a depth equal to 0.63λ. As can be seen in Figure 2b, the depth 0.63λ corresponds closely with the peak of the ridge. The connection with the depth given by 0.63λ demonstrates that the Dix-type relation is a generalized version of the method presented by Xia et al. (1999) for initial model construction. Instead of mapping the shear wave velocity exactly along the depth given by 0.63λ, the regularized inversion based on the Dix-type relation distributes the sensitivity among all depths with the peak sensitivity occurring along the ridge.

We plot the true and inverted depth profiles in Figure 2c. Whereas the true model consists of a sharp interface between the layer and half-space, the regularized inversion finds a smooth model that adequately fits the data. The smooth model captures the overall trend of the true model, with the layer and half-space velocities recovered at shallow and deep levels and the interface smoothed in between. Note that the maximum depth shown in Figure 2c has been determined based on the depth when the diagonal of the resolution matrix, the product of the pseudoinverse of **G** and **G** itself, is at 1% of its peak value. Also shown in Figure 2c are the depth models obtained from the method of Xia et al. (1999) and the underparameterized two-layer method presented previously. We used the phase velocity values from the dispersion curve (including noise) at 3, 8, and 13 Hz for the underparameterized method. Although there is a correspondence in Figure 2b between the mapping used by Xia et al. (1999) and the pseudoinverse, the regularized inversion based on the Dix-type relation generates the more accurate depth model. The underparameterized two-layer method performs best of all, owing to the fact that the true model is a layer over a half-space.

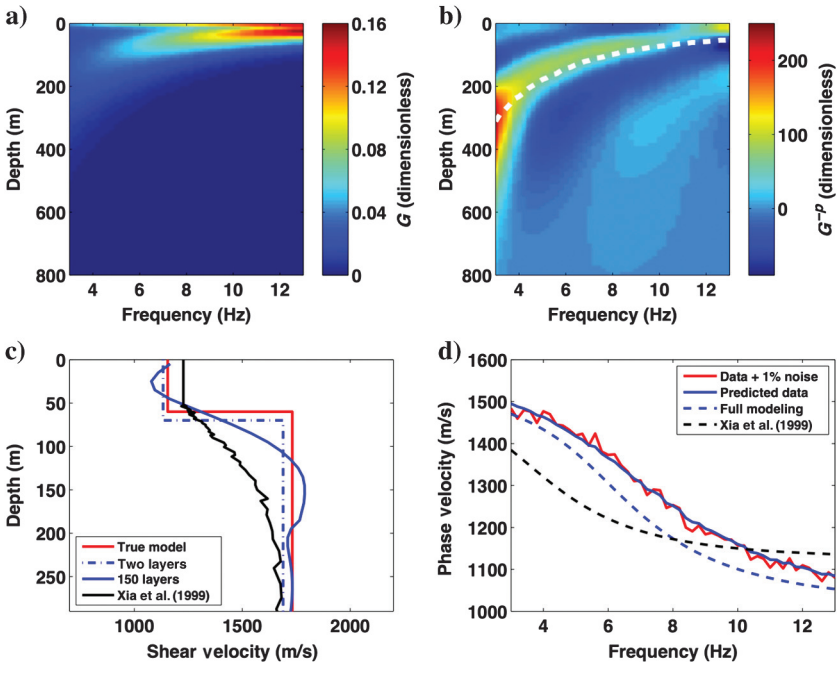

Figure 2. (a) Matrix **G** from equation 12 constructed from synthetic data for a layer-over-a-half-space model, showing the increasing depth sensitivity of surface waves to shear wave velocity at lower frequencies. (b) The regularized pseudoinverse of **G**. Shown as a dashed white line is the depth equal to 0.63λ, in which λ is the wavelength. That depth is the approximate sensitivity depth used by Xia et al. (1999) to construct initial models for surface-wave inversion. (c) The layer-over-a-half-space model (red) and the inversion result (blue). Also shown as a black line is the depth model obtained by the initial model method of Xia et al. (1999). The blue dashed-dotted line is the result of the underparameterized two-layer method discussed in this paper using phase velocities at 3, 8, and 13 Hz. (d) The synthetic data corrupted by 1% noise (red) and the predicted data (blue solid) from the inverted model based on equation 12. Shown in the blue dashed line is the result of full Rayleigh-wave dispersion modeling using the inverted velocity-depth profile in panel (c). The discrepancy between the solid and dashed blue lines represents the additional misfit that can be addressed by nonlinear inversion. The black dashed line is the result of full Rayleigh-wave dispersion modeling using the depth model plotted as a black line in panel (c).

We show the data space in Figure 2d with good agreement between the synthetic data (red) and the predicted data (blue solid) from equation 12 based on the inverted depth model in Figure 2c. However, as discussed previously, equation 12 is an approximation. Full Rayleigh-wave dispersion modeling using the inverted velocity-depth profile (blue curve in Figure 2c) with the thin-layer method, assuming a Poisson's ratio of 0.25 and the Gardner relation for density, results in the exact dispersion curve given by the blue dashed line. The discrepancy between the exact dispersion curve and the dispersion curve predicted from equation 12 can be resolved with subsequent nonlinear inversion using the smooth depth profile in Figure 2c as an initial model. Thus, inversion based on the Dix-type relation is not designed to be a high-precision method, but it can provide a good initial model for further refinement with nonlinear inversion. Moreover, as seen in Figure 2d, the discrepancy between the result of full Rayleigh-wave dispersion modeling is not as pronounced for the Dix-type relation as it is for the initial model generation method of Xia et al. (1999). This further demonstrates that the Dix-type relation is an improved, generalized version of the mapping presented by Xia et al. (1999).

In Figure 3, we compare inversion results for the three Dix-type relations we have derived: Rayleigh waves based on a homogeneous half-space, Rayleigh waves based on power-law velocity profiles, and Love waves based on power-law velocity profiles. The comparisons are done using synthetic data generated for a power-law velocity

profile described by $\beta(z) \sim z^{0.3}$, in which the proportionality is determined by β being equal to 3000 m/s at a depth of 1500 m. As with the inversion results in Figure 2, the synthetic data have been corrupted by 1% noise. All modeling, inversion, and regularization parameters used in Figure 3 are the same as described previously for Figure 2. The constants for the exponential and biexponential approximations of Love- and Rayleigh-wave eigenfunctions are taken from their mean values over the ranges analyzed.

Figure 3a–3c depicts the results for Rayleigh-wave inversion based on a homogeneous half-space, the same type of inversion as is shown in Figure 2. Although based on a homogeneous half-space at each frequency, the inversion performs reasonably well considering the synthetic data are derived from a power-law model, especially between the depths of 50 and 150 m. This may be due in part to the fact that the regularization seeks a smooth model, and power-law velocity profiles are inherently smooth. As observed previously, the ridge of high sensitivity in Figure 3a corresponds closely to the relation 0.63λ. Figure 3d–3f depicts the results for Rayleigh-wave inversion based on power-law velocity profiles. Because the synthetic data are derived from a power-law model, the inversion in this case predictably does better, capturing the entire depth profile more accurately than in Figure 3b. Given the prevalence of power-law velocity profiles in unconsolidated deposits (Godin and Chapman, 2001; Bergamo and Socco, 2013; Tsai and Atiganyanun, 2014), this type of Dix-type relation should be applicable in the shallow subsurface. An interesting feature of the Rayleigh-wave inversion based on power-law velocity profiles is that the ridge of high sensitivity in Figure 3d is closer to 0.5λ than 0.63λ as shown by the black dashed line. This suggests that the depth sensitivity of Rayleigh waves is shallower in power-law velocity profiles than in homogeneous half-space models because the eigenfunctions are more limited in their depth extent. Finally, in panels (g-i) of Figure 3 we show the results for Love waves. In this case, the depth sensitivity is significantly shallower than for Rayleigh waves. The ridge of high sensitivity in Figure 3g is closer to 0.25λ than 0.5λ or 0.63λ as shown by the black dashed line. This suggests that the depth sensitivity of Love waves is shallower in power-law velocity profiles than for Rayleigh waves. Besides the shallower sensitivity, the inversion for Love waves is able to adequately fit the synthetic data and provide a reasonable depth model, albeit over a shorter depth range.

To quantify the error in the Dix-type relation, we plot the nondimensional phase velocity coefficient C_{nd}, described in Appendix A, in Figure 4 for the three cases considered in this paper: Love waves in a power-law profile, Rayleigh waves in a homogeneous profile, and Rayleigh waves in a power-law profile. We also plot C_{nd} for the exact solutions for Rayleigh and Love waves given by Tsai and Atiganyanun (2014). As shown in Appendix A, the Dix-type relation yields identical frequency scaling as the exact solution. Therefore, owing to the scaling properties of phase velocity in power-law profiles, C_{nd} contains all the information needed to fully compare the exact and approximate solutions. The deviation of the approximate solution from the exact solution quantifies the fractional error introduced by the Dix-type relation. In Figure 4, the Dix-type relation for Rayleigh waves in a homogeneous profile produces estimates of phase velocity that converge to the exact solution at small values of the exponent describing the depth dependence α. This behavior is expected because the depth profile becomes more homogeneous at small α. At $\alpha = 0.3$, the homogeneous Dix-type relation overestimates the true phase velocity by approximately 20%, in agreement with panels (b and c) in Figure 3. For $\alpha > 0.3$, the homogeneous Dix-type relation is not a satisfactory approximation and the power-law Dix-type relation for Rayleigh waves can be used because it fits the exact solution over a wide range of α. Similarly, the power-law Dix-type relation for Love waves fits the exact solution over a wide range.

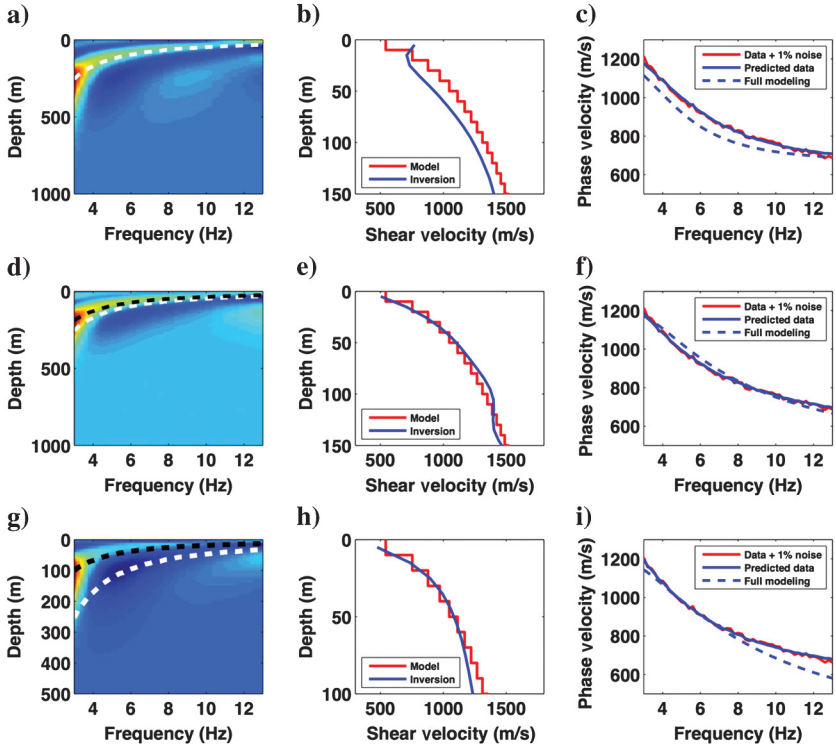

Figure 3. Performance of Rayleigh- and Love-wave inversion based on the Dix-type relation with velocity models that have power-law variation with depth. (a) Regularized pseudoinverse for Raleigh-wave inversion with approximate eigenfunctions taken from a homogeneous model. The depth 0.63λ is given by a white dashed line as in Figure 2b. (b) The power-law model (red) and the inversion result (blue). (c) The synthetic data corrupted by 1% noise (red) and the predicted data (blue solid) from the inverted model based on equation 12. Shown as a blue dashed line are the predicted data from the inverted model using full forward modeling of surface-wave dispersion. Panels (d-f) are the same as panels (a-c) except that the approximate eigenfunctions are based on fitting the eigenfunctions from a family of power-law models with a biexponential model as described in Table 1. The depths 0.63λ and 0.5λ are given by white dashed and black lines, respectively. Panels (g-i) are the same as panels (d-f) but are for the case of Love waves instead of Rayleigh waves. The depth 0.25λ is given by a black dashed line with 0.63λ given by a white dashed line.

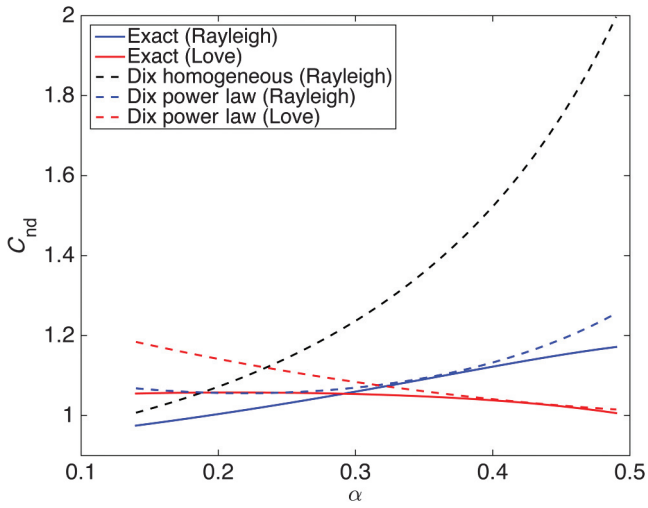

Figure 4. Quantification of the error introduced by the approximate Dix-type relations. Shown are nondimensional phase velocity coefficient C_{nd} versus power-law exponent α for the three cases considered in this article: Love waves in a power-law profile (red dashed line), Rayleigh waves in a homogeneous profile (black dashed line), and Rayleigh waves in a power-law profile (blue dashed line). Exact results (Tsai and Atiganyanun, 2014) for Rayleigh and Love waves are given by blue and red lines, respectively.

NEAR-SURFACE EXAMPLE

To demonstrate that the Dix-type relation is capable of generating accurate velocity profiles in the near surface, we have processed a benchmark data set from the National Geotechnical Experimentation Site (NGES) at Texas A&M University (Michaels, 2011). These data were provided to the community by the American Society of Civil Engineers (ASCE) in 2010 to test surface-wave inversion methods. The data set, shown in Figure 5a, consists of 62 geophones placed at 2-ft intervals with an inner offset of 40 ft. From this receiver geometry, we compute the phase-velocity spectrum in Figure 5b and pick the peak at each frequency to construct the measured dispersion curve.

We setup an inversion similar to the example shown in Figure 2, using the homogeneous medium formulation to define f as shown in equation 10. The model consists of 250 layers, with all layers being 0.25-m thick except for the bottom layer, which extends to infinite depth. With the NGES data and the inversion model, we construct the matrix $\mathbf{G}$ as in equation 12 as shown in Figure 5c. We take the data and model standard deviations in equations 26 and 27 to correspond with velocities of 5 and 10 m/s, respectively, and we use a smoothing length of 1 m. With these regularization parameters, the pseudoinverse plotted in Figure 5d has a similar appear-

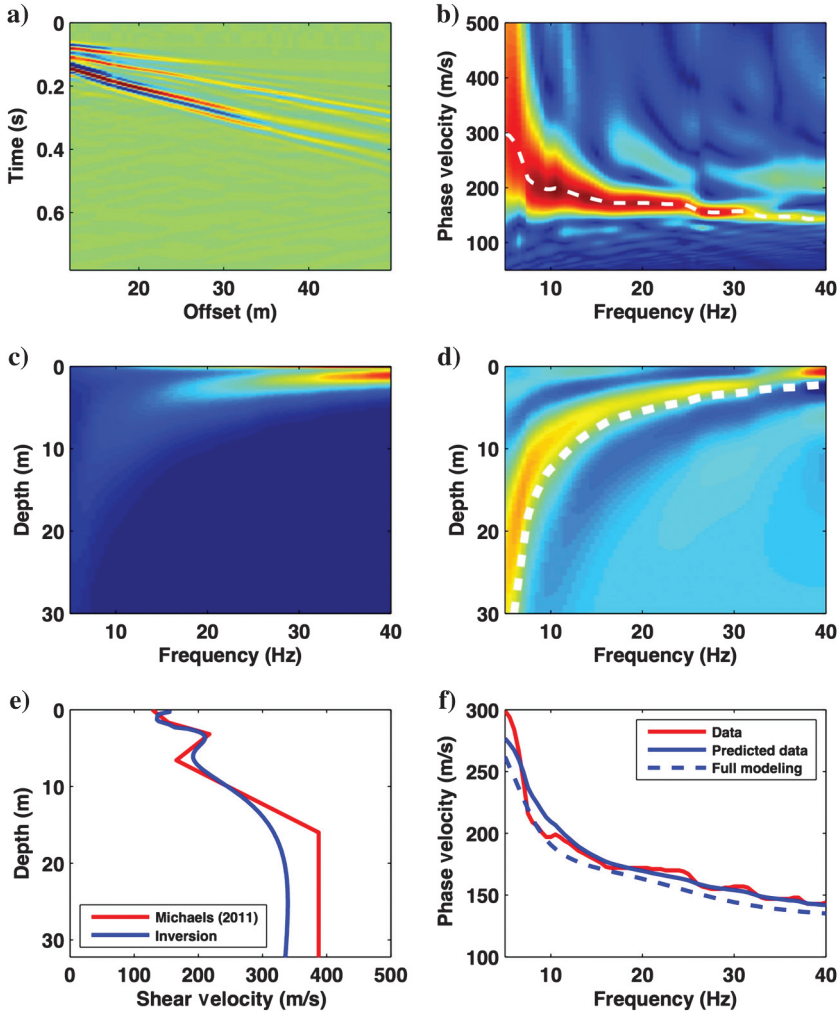

Figure 5. Application of inversion based on the Dix-type relation in a near-surface setting. (a) Data set from the NGES. (b) Measured phase-velocity curve (white dashed line) overlain on the phase-velocity spectrum. (c) Matrix $\mathbf{G}$ from equation 12 constructed from the measured phase velocity. (d) The regularized pseudoinverse of $\mathbf{G}$. Shown as a white dashed line is the depth equal to 0.63λ, in which λ is the wavelength. (e) The inversion result (blue) and the depth model (red) obtained by Michaels (2011) for the NGES data using iterative nonlinear inversion. The Dix-type inversion recovers several of the features of the Michaels (2011) depth model, including the velocity reversal between 3- and 7-m depth. (f) The measured phase-velocity curve (red) and the predicted data (blue solid) from the inverted model based on equation 12. Shown as a blue dashed line is the result of full Rayleigh-wave dispersion modeling using the inverted velocity-depth profile in panel (e).

ance to the previous examples with a relatively compact ridge extending to depths of 30 m as frequency decreases.

We plot the inversion result in Figure 5e along with the depth profile obtained by Michaels (2011) using standard, iterative phase-velocity inversion. As can be seen, the Dix-type relation is able to recover several of the same features as the result from Michaels (2011). Most notable is the velocity reversal between 3 and 7 m depth. This shows that, for this near-surface data set, the approximation inherent in the Dix-type relation is not a severe limitation. Figure 5f further bears out the accuracy of the Dix-type relation for this data set, with the predicted data and dispersion curve from full modeling in reasonably close agreement with each other.

DISCUSSION

In light of the connection we have found between the Dix-type relation for surface waves and the initial model construction method of Xia et al. (1999), it is instructive to return to the underparameterized inversion data example in Figure 1 and investigate why it worked so well. Recall that, in the example, we used phase velocities measured at periods of 8, 20, and 40 s. Owing to the 0.63λ depth sensitivity pointed out by Xia et al. (1999) and further demonstrated by the pseudoinverse in Figure 2b, phase velocities at these periods are sensitive to depths of 18, 44, and 88 km assuming a nominal Rayleigh-wave phase velocity of 3.5 km/s at these periods. These sensitivity depths bracket the average depth of the Moho, 35 km. Therefore, using this period range is well suited for resolving properties of the crust and upper mantle simultaneously from surface waves. Note that using precise Rayleigh-wave phase velocities at these periods instead of the approximation of 3.5 km/s to find the sensitivity depth does not change the overall picture. Thus, the depth sensitivity of 0.63λ can be used to determine, a priori, a set of three phase-velocity measurements suitable for resolving a surface waveguide of a given thickness above a lower half-space.

In addition to the connection with the 0.63λ sensitivity depth, we have also obtained results on the sensitivity depth of Rayleigh and Love waves in velocity profiles in which the shear wave velocity obeys a power law. In power-law velocity profiles, the sensitivity depth is reduced relative to a homogeneous medium, and the Love-wave sensitivity is significantly shallower than the Rayleigh-wave sensitivity. We plan to address more details of surface-wave inversion beyond the scope of phase velocities for fundamental-mode Rayleigh and Love waves in the future. For example, it remains to be seen if the Dix-type relation can be extended to group velocities and higher modes, especially in the presence of Poisson's ratio variations in depth. Although the result with the NGES data set is promising, more testing of the Dix-type relation with near-surface data sets is necessary to establish its effectiveness. Of particular interest is the use of the surface-wave Dix-type relation to process ground roll in exploration seismic surveys for obtaining near-surface shear wave velocities (Haney and Douma, 2012; Douma and Haney, 2013). At the continental scale, we also plan to apply the underparameterized method for large-scale mapping of the Moho in regions with existing surface-wave phase velocity maps.

CONCLUSIONS

We have extended the principles underlying the well-known Dix equation in reflection seismology to surface waves. We discussed the under- and overparameterized formulations of the inverse problem and extended the theory from homogeneous to power-law velocity profiles to include Love waves and improve the approximation for Rayleigh waves. For the underparameterized formulation, we applied the theory to invert for crustal thickness, crustal shear velocity, and upper-mantle shear velocity across the western United States from only three phase velocity measurements. We made strong connections between the Dix-type relation and an existing method for constructing initial models directly from Rayleigh-wave data. Our results indicate that the Dix formalism is valid for surface waves and constitutes a reliable way for constructing approximate velocity models directly from surface-wave dispersion data. The Dix-type relation has also shed light on the depth sensitivity of surface-wave dispersion data in a quantitative way based on the analysis of the pseudoinverse matrix mapping squared phase velocities into squared layer shear velocities. Finally, we tested the methodology by processing a benchmark near-surface data set and found good agreement between the inversion result based on the Dix-type relation and a published depth profile generated with classical surface-wave inversion.

ACKNOWLEDGMENTS

The authors wish to thank F.-C. Lin for providing access to the phase velocity maps of the western United States. They also thank assistant editor V. Socco, associate editor G. Tsoflias, P. Dawson, and three anonymous reviewers for their helpful comments.

APPENDIX A

DIX-TYPE RELATION FOR A CONTINUOUSLY LAYERED MEDIUM AND POWER-LAW SCALING

Equation 11 states that

$$c_m^2 = \sum_{n=1}^{N} [f(k_m, h_{n+1}) - f(k_m, h_n)]\beta_n^2. \tag{A-1}$$

Denoting the quantity in brackets in the above equation as Δf_n and the depth interval $h_{n+1} - h_n$ as Δh_n, equation 11 can be rewritten as

$$c_m^2 = \sum_{n=1}^{N} \frac{\Delta f_n}{\Delta h_n} \beta_n^2 \Delta h_n, \tag{A-2}$$

which is recognized as a Riemann sum whose limit for infinitesimally thin layers is the integral

$$c^2(\omega) = \int_0^{\infty} \frac{\partial f(k,z)}{\partial z} \beta^2(z) dz, \tag{A-3}$$

in which $k = \omega/c$. We now consider shear velocity profiles described by a power law of the form:

$$\beta(z) = \beta_0 \left(\frac{z}{z_0}\right)^{\alpha}. \tag{A-4}$$

We also consider functions f that are generally represented as a sum of J exponentials

$$f(k,z) = \sum_{j=1}^{J} a_j e^{-b_j k z} \tag{A-5}$$

with coefficients a_j and b_j. This general form covers the three cases considered in this article: Love waves in a power-law profile ($J = 1$), Rayleigh waves in a homogeneous profile ($J = 3$), and Rayleigh waves in a power-law profile ($J = 10$). The derivative of f with respect to z is given by

$$\frac{\partial f(k,z)}{\partial z} = -k \sum_{j=1}^{J} a_j b_j e^{-b_j k z}. \tag{A-6}$$

Substituting equations A-4 and A-6 into equation A-3 yields

$$c^2 = -k \sum_{j=1}^{J} a_j b_j \beta_0^2 z_0^{-2\alpha} \int_0^{\infty} e^{-b_j k z} z^{2\alpha} dz. \tag{A-7}$$

The integral in equation A-7 is a Laplace transform given by

$$\int_0^{\infty} e^{-b_j k z} z^{2\alpha} dz = \frac{\Gamma(1+2\alpha)}{(b_j k)^{2\alpha+1}}. \tag{A-8}$$

Substituting this expression and the relation $k = \omega/c$ into equation A-7 results in

$$c^2 = -\beta_0^2 z_0^{-2\alpha} \omega^{-2\alpha} c^{2\alpha} \Gamma(1+2\alpha) \sum_{j=1}^{J} a_j b_j^{-2\alpha}. \tag{A-9}$$

Taking the square root of both sides of equation A-9 yields

$$c = \beta_0 z_0^{-\alpha} \omega^{-\alpha} c^{\alpha} \left[-\Gamma(1+2\alpha) \sum_{j=1}^{J} a_j b_j^{-2\alpha} \right]^{\frac{1}{2}}. \tag{A-10}$$

We group all c terms on the left side of equation A-10 and introduce a reference frequency ω_0. This produces the following expression:

$$c^{1-\alpha} = \frac{\beta_0}{(z_0 \omega_0)^{\alpha}} \left(\frac{\omega}{\omega_0} \right)^{-\alpha} \left[-\Gamma(1+2\alpha) \sum_{j=1}^{J} a_j b_j^{-2\alpha} \right]^{\frac{1}{2}}. \tag{A-11}$$

Finally, inverting the power on the c term on the left side of equation A-11 gives the expression

$$c = \left[\frac{\beta_0}{(z_0 \omega_0)^{\alpha}} \right]^{\frac{1}{1-\alpha}} \left(\frac{\omega}{\omega_0} \right)^{-\frac{\alpha}{1-\alpha}} \left[-\Gamma(1+2\alpha) \sum_{j=1}^{J} a_j b_j^{-2\alpha} \right]^{\frac{1}{2(1-\alpha)}}, \tag{A-12}$$

in which the first term on the right side has the physical dimension of velocity and the remaining two terms are dimensionless. Note that the Dix-type relation has the same frequency scaling as the exact solution (Tsai and Atiganyanun, 2014). Following Tsai and Atiganyanun (2014), we refer to the third term on the right side of equation A-12 as the nondimensional phase velocity coefficient

$$C_{nd} = \left[-\Gamma(1+2\alpha) \sum_{j=1}^{J} a_j b_j^{-2\alpha} \right]^{\frac{1}{2(1-\alpha)}}, \tag{A-13}$$

which is plotted in Figure 4.

REFERENCES

Aki, K., and P. G. Richards, 1980, Quantitative seismology: W. H. Freeman and Company.

Aster, R., B. Borchers, and C. Thurber, 2004, Parameter estimation and inverse problems: Elsevier/Academic Press.

Bergamo, P., and L. V. Socco, 2013, Estimation of P- and S-wave velocity of unconsolidated granular materials through surface wave multimodal inversion: 83rd Annual International Meeting, SEG, Expanded Abstracts, 1776–1779.

Chulick, G. S., and W. D. Mooney, 2002, Seismic structure of the crust and uppermost mantle of North America and adjacent oceanic basins: A synthesis: Bulletin of the Seismological Society of America, **92**, 2478–2492, doi: 10.1785/0120010188.

Dix, C. H., 1955, Seismic velocities from surface measurements: Geophysics, **20**, 68–86, doi: 10.1190/1.1438126.

Douma, H., and M. M. Haney, 2013, Exploring non-linearity and non-uniqueness in surface-wave inversion for near-surface velocity estimation: The Leading Edge, **32**, 648–655, doi: 10.1190/tle32060648.1.

Evison, F. F., R. H. Orr, and C. E. Ingham, 1959, Thickness of the Earth's crust in Antarctica: Nature, **183**, 306–308, doi: 10.1038/183306a0.

Gardner, G. H. F., L. W. Gardner, and A. R. Gregory, 1974, Formation velocity and density — The diagnostic basis for stratigraphic traps: Geophysics, **39**, 770–780, doi: 10.1190/1.1440465.

Gerstoft, P., K. G. Sabra, P. Roux, W. A. Kuperman, and M. C. Fehler, 2006, Green's functions extraction and surface-wave tomography from microseisms in southern California: Geophysics, **71**, no. 4, SI23–SI31, doi: 10.1190/1.2210607.

Godin, O., and D. M. F. Chapman, 2001, Dispersion of interface waves in sediments with power-par shear speed profiles. I. Exact and approximate analytical results: Journal of the Acoustical Society of America, **47**, 117–148, doi: 10.1121/1.1401776.

Grechka, V., I. Tsvankin, and J. K. Cohen, 1999, Generalized Dix equation and analytic treatment of normal-moveout velocity for anisotropic media: Geophysical Prospecting, **47**, 117–148, doi: 10.1046/j.1365-2478.1999.00120.x.

Haney, M. M., K. T. Decker, and J. H. Bradford, 2010, Permittivity structure derived from group velocities of guided GPR pulses, *in* R. D. Miller, J. H. Bradford, and K. Holliger, eds., Advances in near surface seismology and ground penetrating radar: SEG, 167–184.

Haney, M. M., and H. Douma, 2012, Rayleigh wave tomography at Coronation Field, Canada: The topography effect: The Leading Edge, **31**, 54–61, doi: 10.1190/1.3679328.

Harlan, W. S., 1999, Constrained Dix inversion. http://billharlan.com/pub/papers/rmsinv.pdf, accessed 8 September 2015.

Kausel, E., 2005, Waves propagation modes: From simple systems to layered soils, *in* C. G. Lai, and K. Wilmanski, eds., Surface waves in geomechanics: Direct and inverse modelling for soil and rocks: Springer-Verlag, 165–202.

Kennett, B. L. N., and E. R. Engdahl, 1991, Traveltimes for global earthquake location and phase identification: Geophysical Journal International, **105**, 429–465, doi: 10.1111/j.1365-246X.1991.tb06724.x.

Koren, Z., and I. Ravve, 2006, Constrained Dix inversion: Geophysics, **71**, no. 6, R113–R130, doi: 10.1190/1.2348763.

Lay, T., and T. C. Wallace, 1995, Modern global seismology: Academic Press.

Lin, F.-C., M. P. Moschetti, and M. H. Ritzwoller, 2008, Surface wave tomography of the western United States from ambient seismic noise: Rayleigh and Love wave phase velocity maps: Geophysical Journal International, **173**, 281–298, doi: 10.1111/j.1365-246X.2008.03720.x.

Lin, F.-C., M. H. Ritzwoller, and R. Snieder, 2009, Eikonal tomography: Surface wave tomography by phase-front tracking across a regional broad-band seismic array: Geophysical Journal International, **177**, 1091–1110, doi: 10.1111/j.1365-246X.2009.04105.x.

Lysmer, J., 1970, Lumped mass method for Rayleigh waves: Bulletin of the Seismological Society of America, **60**, 89–104.

Michaels, P., 2011, Establishing confidence in surface wave determined soil profiles, *in* C. H. Juang, K. K. Phoon, A. J. Puppala, R. A. Green, and G. A. Fenton, eds., Geo-Risk 2011: Risk assessment and management (GSP 224): American Society of Civil Engineers, 837–844.

Snieder, R., and J. Trampert, 1999, Inverse problems in geophysics, *in* A. Wirgin, ed., Wavefield inversion: Springer Verlag, 119–190.

Stewart, R. R., and R. J. Ferguson, 1997, Shear-wave interval velocity from P-S stacking velocities: Canadian Journal of Exploration Geophysics, **32**, 139–142.

Taner, M. T., and F. Koehler, 1969, Velocity spectra — Digital computer derivation and applications of velocity functions: Geophysics, **34**, 859–881, doi: 10.1190/1.1440058.

Tsai, V. C., and S. Atiganyanun, 2014, Green's functions for surface waves in a generic velocity structure: Bulletin of the Seismological Society of America, **104**, 2573–2578, doi: 10.1785/0120140121.

Tsai, V. C., B. Minchew, M. P. Lamb, and J.-P. Ampuero, 2012, A physical model for seismic noise generation from sediment transport in rivers: Geophysical Research Letters, **39**, L02404, doi: 10.1029/2011GL050255.

Xia, J., R. D. Miller, and C. B. Park, 1999, Estimation of near-surface shear-wave velocity by inversion of Rayleigh waves: Geophysics, **64**, 691–700, doi: 10.1190/1.1444578.

Yilmaz, Ö., 1987, Seismic data processing: SEG.